Supplement

Angharad C. Stell, Luke M. Western, Matthew Rigby

1 Loss kinetic isotope effect range

The isotopic fractionation is described by the kinetic isotope effect (KIE), which is defined as

$$\text{KIE} = \frac{k_{12}}{k_{13}}, \tag{1}$$

where k_{12} is the reaction rate constant of $^{12}CH_4$ and k_{13} is the reaction rate constant of $^{13}CH_4$. The KIEs used in MOZART are presented in Table S1. These values are derived from the literature, which are summarised in this section.

The stratospheric loss KIE is calculated by weighting the contribution of Cl and O(^{1}D) to stratospheric methane loss by the ratio given in Saunois et al. (2016), and the soil loss is modelled as negative emissions with isotopic fractionation calculated similarly to Lassey et al. (2007).

Table S1: The one standard deviation range of KIEs examined in the MOZART model.

	Minimum	Maximum	Default value
$^{13C}\text{KIE}_{OH}$	1.0037	1.0041	1.0039
$^{13C}\text{KIE}_{STRAT}$	1.035	1.044	1.0402
$^{13C}\text{KIE}_{Cl}$	1.0635	1.0665	1.065
$^{13C}\text{KIE}_{soil}$	1.0185	1.0235	1.021

1.1 Reaction of CH$_4$ and OH

The range of literature values for the reaction of CH_4 and OH are presented in Table S2. Rust and Stevens (1980) had experimental difficulties and recorded a large range of values (1.0003 to 1.0078) and Davidson et al. (1987) was superseded by Cantrell et al. (1990). This leaves only Saueressig et al. (2001) and Cantrell et al. (1990). In this work, the two standard deviation range is taken as $^{13C}\text{KIE}_{OH}$=1.0035-1.0043, from the accepted value of Saueressig et al. (2001).

Table S2: Literature values reported for the kinetic isotope effect of CH$_4$ and OH.

	Reference	KIE	Two standard deviations
Experimental	Saueressig et al. (2001)	1.0039	0.0004
	Cantrell et al. (1990)	1.0054	0.0009
	Davidson et al. (1987)	1.010	0.007
	Rust and Stevens (1980)	1.0036	0.0026
Theoretical	Gupta et al. (1997)	1.010	
	Melissas and Truhlar (1993)	1.005	
	Lasaga and Gibbs (1991)	1.007	

1.2 Reaction of CH_4 and $O(^1D)$

There are very few studies of the KIE of the reaction of CH_4 and $O(^1D)$: Saueressig et al. (2001) report a value of 1.013, whereas Davidson et al. (1987) report a value of 1.001 from a single experiment. In this work, we take only the accepted value from Saueressig et al. (2001), which the authors report as having a negligible uncertainty.

1.3 Reaction of CH_4 and Cl

Table S3 shows the literature range of values for $^{13C}KIE_{Cl}$. There is good agreement between the experimental literature values. The full range of the two standard deviation uncertainty of these experimental studies was taken, to give a range of 1.062 to 1.068.

Table S3: Literature values reported for the kinetic isotope effect of CH_4 and Cl.

	Reference	KIE	Two standard deviations
Experimental	Tyler et al. (2000)	1.0621	0.0001
	Crowley et al. (1999)	1.066	0.002
	Saueressig et al. (1995)	1.066	0.002
Theoretical	Roberto-Neto et al. (1998)	1.06	
	Gupta et al. (1997)	1.034	
	Tanaka et al. (1997)	1.026	

1.4 Loss of CH_4 by soil

The literature values of $^{13C}KIE_{soil}$ are shown in Table S4. There is good agreement between these studies and so the full range of values are used, giving a two standard deviation range of 1.016 to 1.026.

Table S4: Literature values reported for the kinetic isotope effect of CH_4 and soil.

Reference	KIE	Two standard deviations
Snover and Quay (2000)	1.0173	0.0020
	1.0181	0.0008
Reeburgh et al. (1997)	1.023	
	1.026	
Tyler et al. (1994)	1.022	0.008
King et al. (1989)	1.026	
	1.016	

2 Freshwater emissions dataset

In this work, the Global Lakes and Wetlands Database (GLWD) (Lehner and Döll, 2004) was used to create a global emissions dataset of freshwater bodies. The methane emissions from a freshwater body was weighted according to its percentage of the global freshwater area, to give a global total of 120 $Tg\,yr^{-1}$ (Saunois et al., 2016). The Earth was split into three latitude bands: tropical (less than 30 ° N and S), mid-latitudes (30-50 ° N and S), and high-latitudes (more than 50 ° N and S), and weighted according to Saunois et al. (2016) to account for the different climatic conditions: 49

% tropical, 33 % mid-latitudes, and 18 % high-latitudes. The emissions map is time-invariant due to a lack of observational evidence (Natchimuthu et al., 2016; Wik, Thornton, Bastviken, Uhlbäck and Crill, 2016), but it is possible that freshwater emissions have a large seasonal cycle due to the dependency on temperature (Wilkinson et al., 2015). The resulting freshwater emissions distribution can be seen in Fig. S1, and the NetCDF file (along with the code used to create it) is available to be downloaded at https://doi.org/10.17605/OSF.IO/Q9F8P (Stell, 2020).

There are several improvements that could be made to the freshwater emissions dataset. The first is to use a power law to describe the relationship between the freshwater body area and methane emissions (e.g. Bastviken et al. (2004); Wik, Varner, Anthony, MacIntyre and Bastviken (2016)). This relationship means that the many small water bodies missing from GLWD are important (Holgerson and Raymond, 2016), and ideally lakes from the higher resolution GLObal WAter BOdies database (GLOWABO) (Verpoorter et al., 2014) should be included. Additionally, more careful consideration of which bodies to include might be beneficial, for example, the Caspian Sea is somewhat saline and so could be reduced or removed from the map (e.g. Liu and Boone (1991); Pattnaik et al. (2000)). Lake depth is also a key variable in predicting methane emissions from ebullition (Bastviken et al., 2004). Lake depths for the largest lakes are included in Kourzeneva et al. (2012), so there is potential to combine all available databases to extract as much information as possible. Variables such as temperature, water body type, and altitude would also ideally be included. The suggested improvements to the freshwater emission dataset are not required for this work, as the map is latitude-band weighted, so the hemispheric distribution is correct. As this work only uses hemispheric data, this will not majorly impact the results.

Methane flux / Tg yr^{-1}
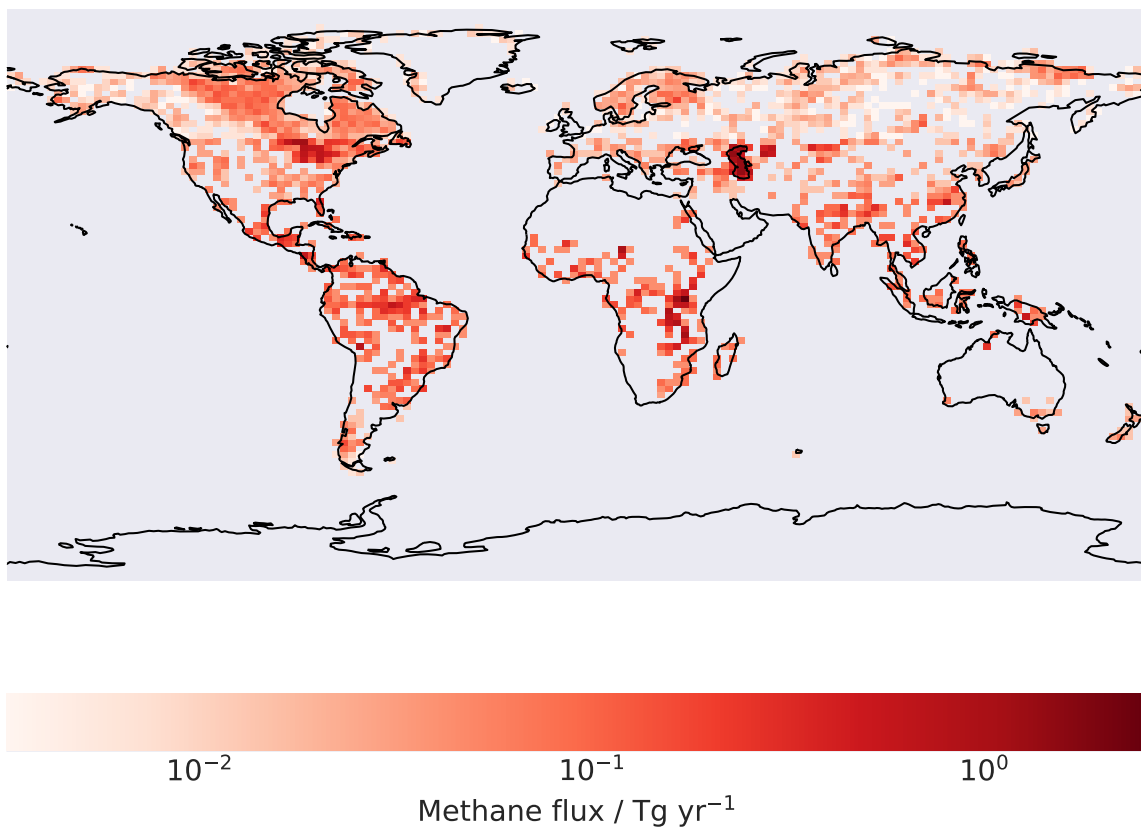
Figure S1: The global distribution of freshwater methane emissions used in this work. Total methane emissions are 120 Tg yr^{-1} (Saunois et al., 2016), which is distributed according to the freshwater area in three latitude bands as described in the text.

3 Emulator Validation

3.1 Relation between emulator errors and inputs

Differences between the emulator prediction and the true model should not correlate with the input values. If correlations are present, this indicates that either some emulator parameters are not optimal or non-stationarity (Bastos and O'Hagan, 2009). In Fig. S2, Fig. S3, Fig. S4, and Fig. S5, the difference between the mean of the prediction for the emulators and the true model value for the validation dataset are plotted against each input parameter value in a separate panel. There is no correlation between any emulator and any input parameter.
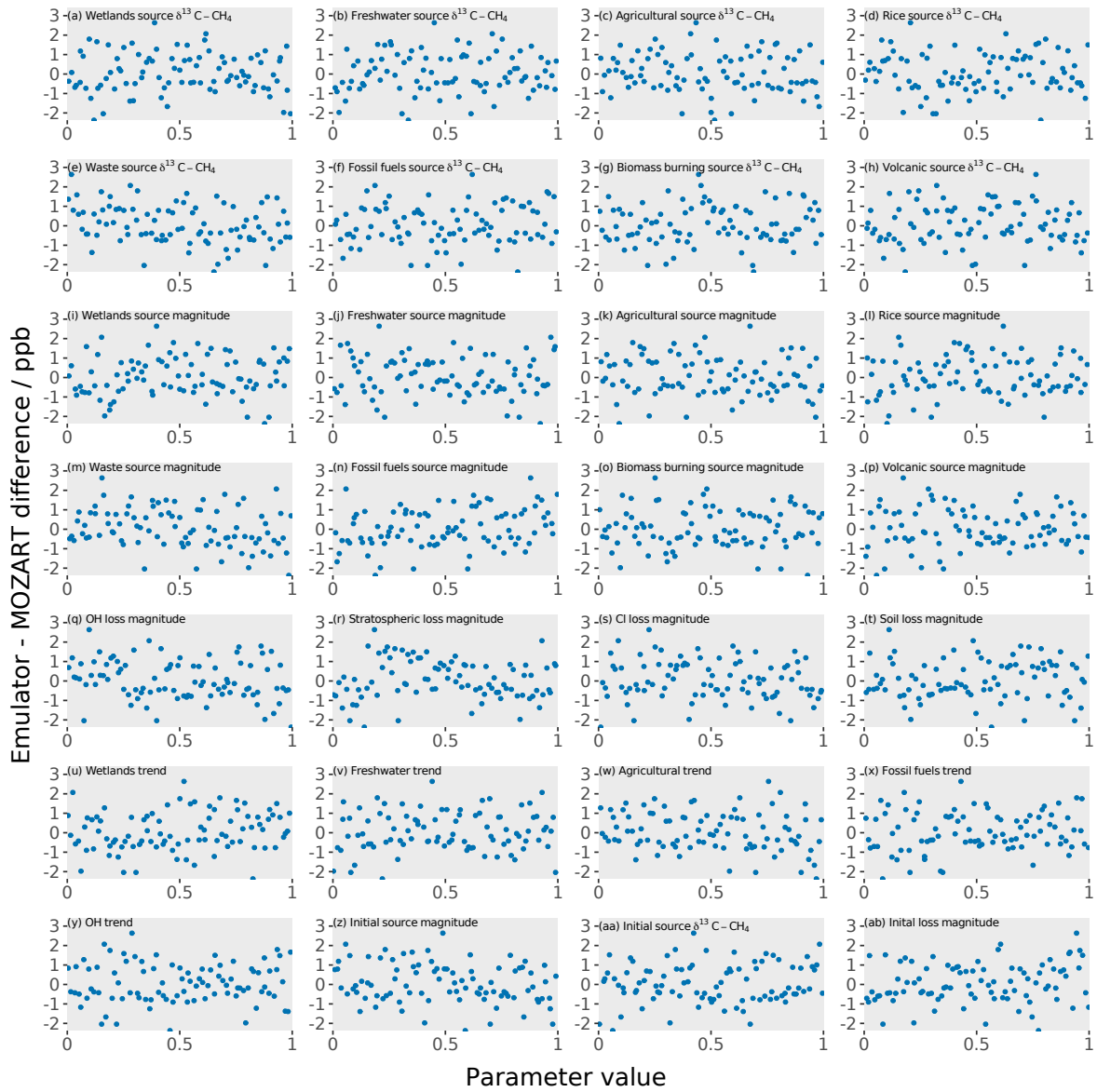
Figure S2: The difference between the southern hemisphere mole fraction emulator and the true value in the MOZART model is plotted against each input parameter.
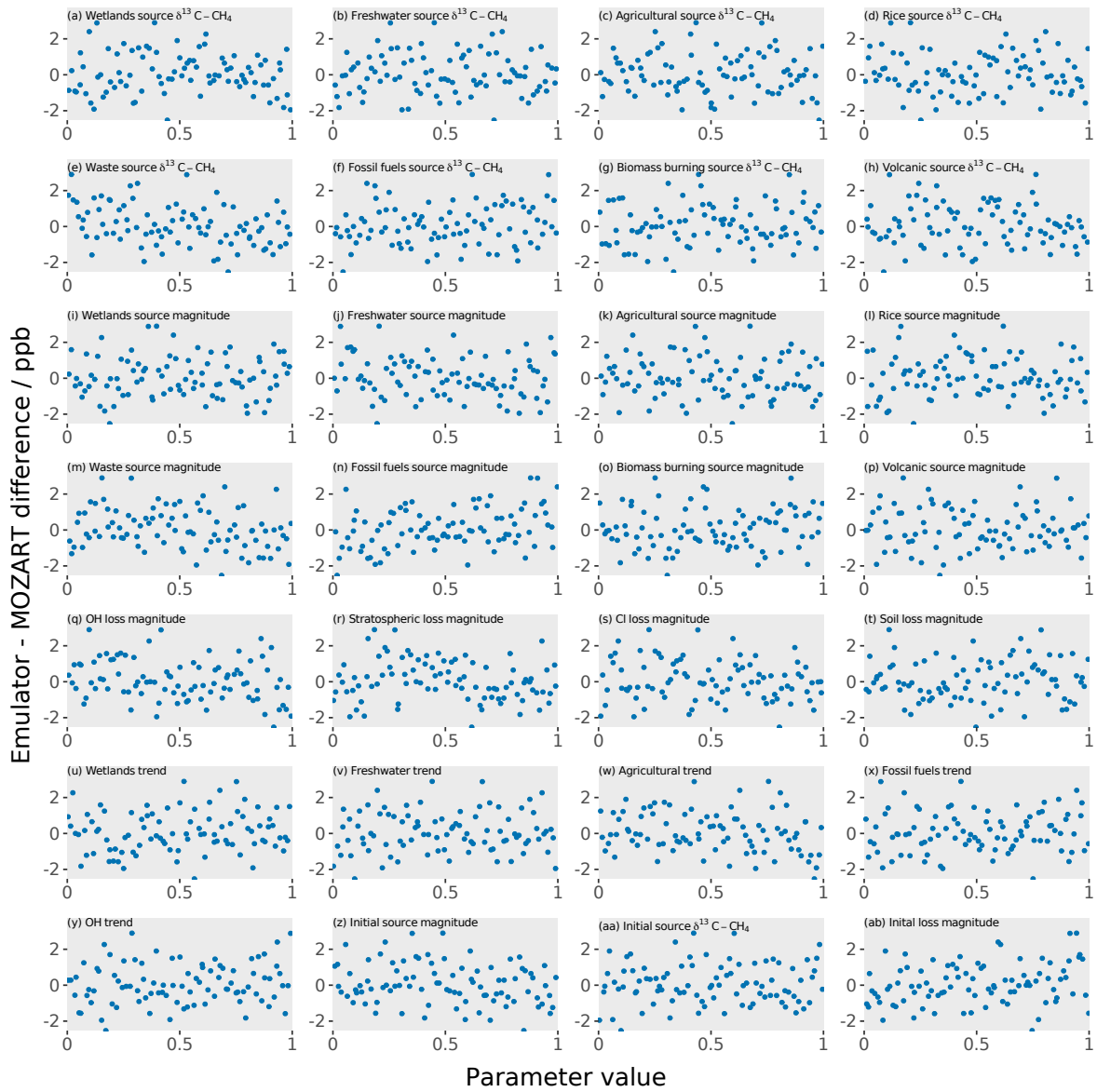
Figure S3: The difference between the northern hemisphere mole fraction emulator and the true value in the MOZART model is plotted against each input parameter.
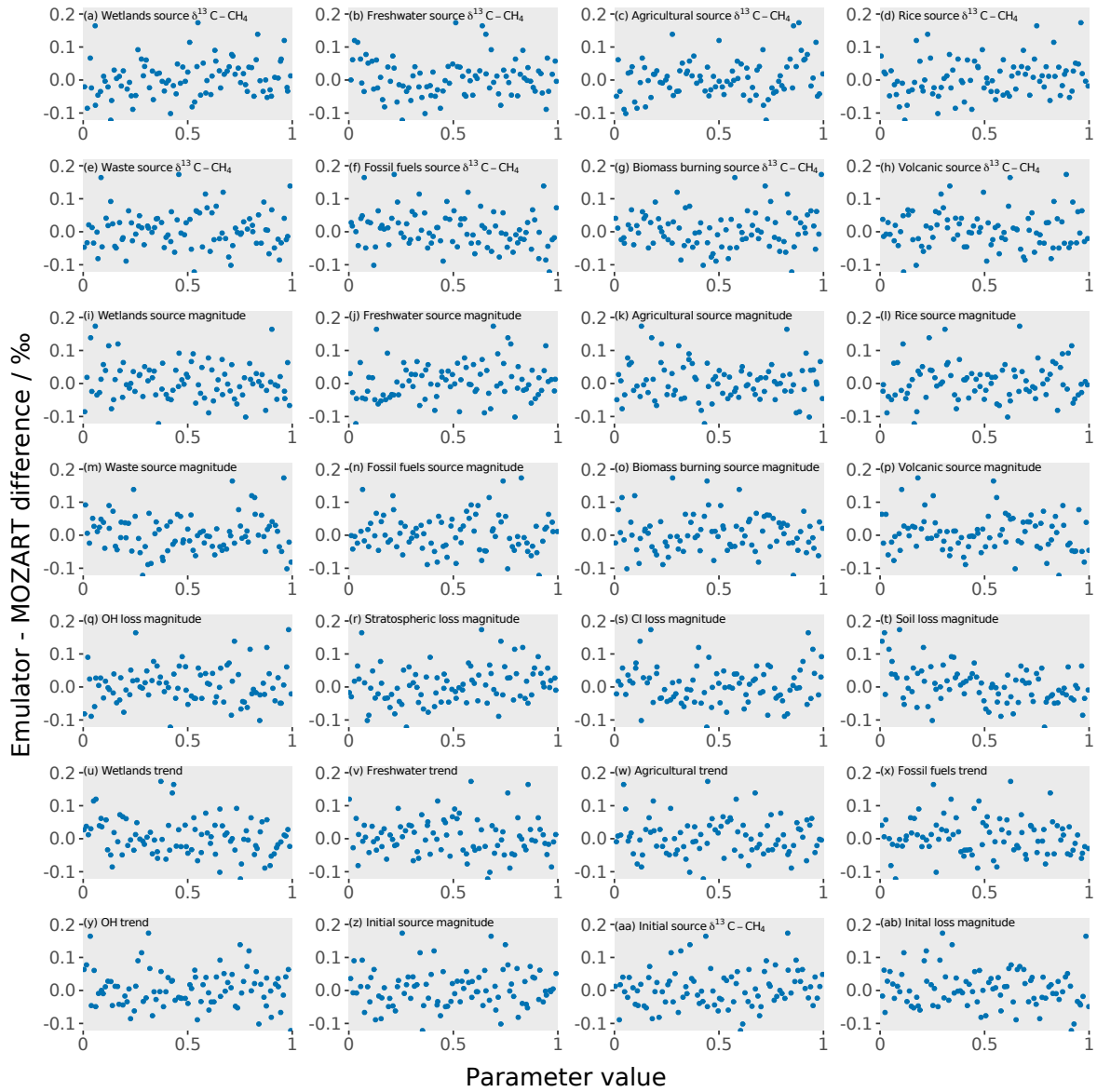
Figure S4: The difference between the southern hemisphere δ^{13}C-CH$_4$ emulator and the true value in the MOZART model is plotted against each input parameter.
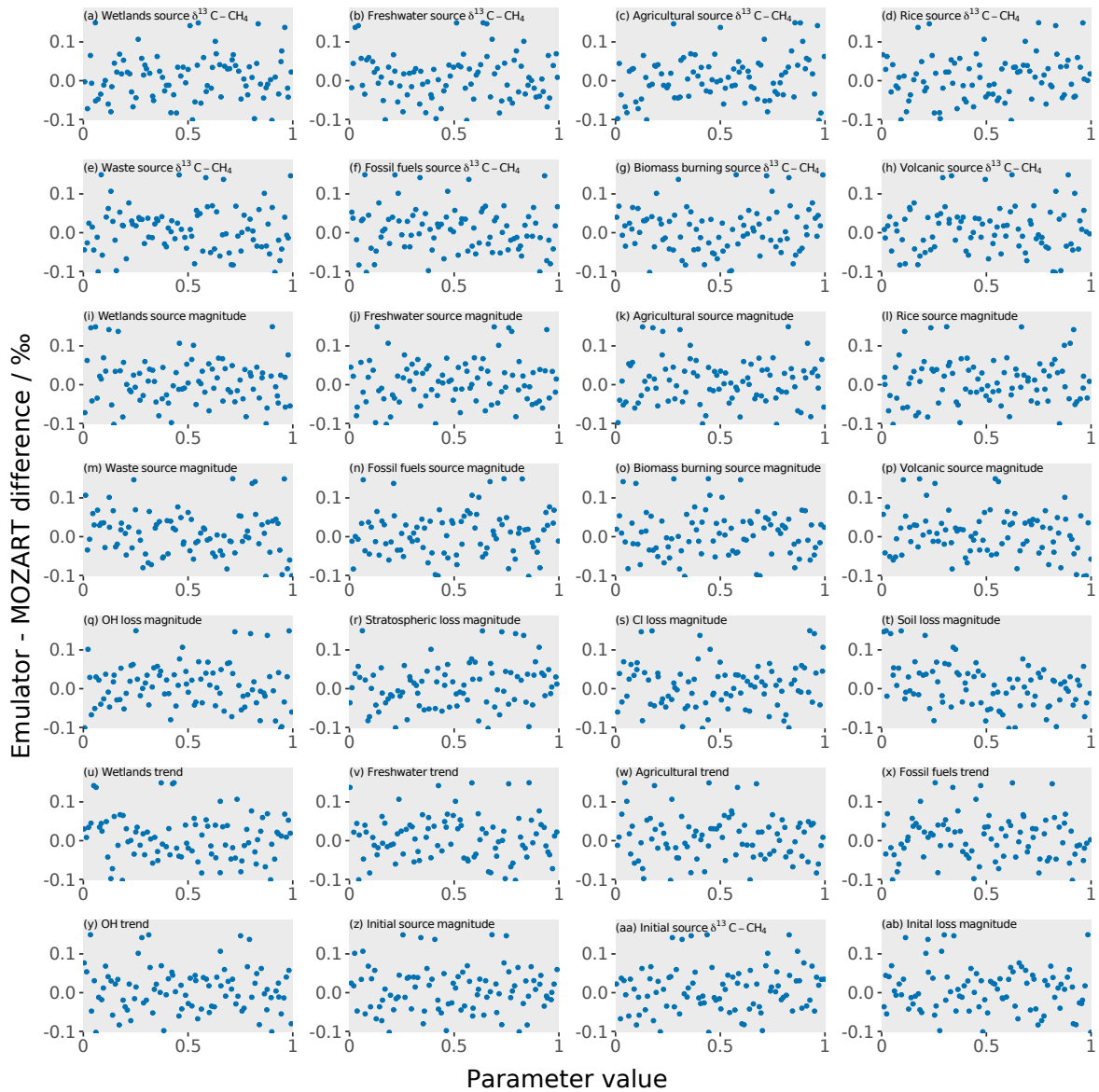
Figure S5: The difference between the northern hemisphere δ^{13}C-CH$_4$ emulator and the true value in the MOZART model is plotted against each input parameter.

3.2 Relation between emulator errors and outputs

Standardised residuals between the emulator and the true model simulation in the validation dataset should also be normally distributed. These residuals are calculated by

$$\epsilon = \frac{y_{em} - y_{mzt}}{\sigma_{em}}, \tag{2}$$

where y_{em} is the emulator prediction for one month, y_{mzt} is the corresponding MOZART output, and σ_{em} is the emulator calculated error for that month. These residuals are compared to a normal distribution in Fig. S6. The residuals are close to normally distributed, with the largest difference for the mole fraction emulators in the middle of the time series. Here the emulator error is larger than that

seen in the residuals. This is because the emulator estimated error is time-invariant (as the emulator error only depends on the difference between the inputs), but the model output range is smaller in the middle of the time series due to the design of the trend parameters. The trend parameters conserve the total magnitude of the source or sink over the time series. Therefore, all the possible trend values have the same magnitude in the centre of the time series, so there is a smaller output range here. This effect is not seen in the δ^{13}C-CH$_4$ emulators due to the longer time between input changes and δ^{13}C-CH$_4$ response.
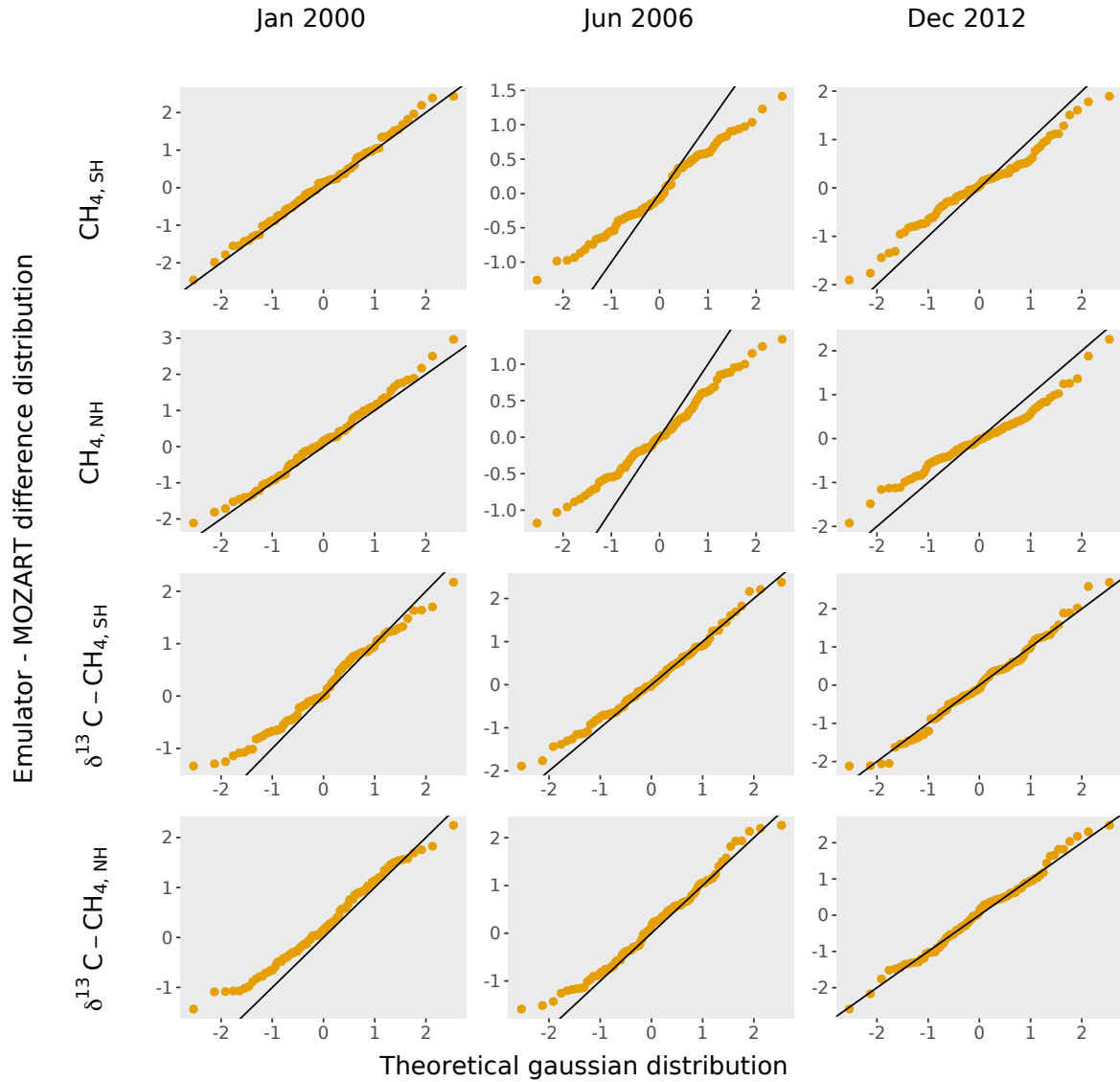
Figure S6: Quantile-quantile plots of the standardised emulator residuals for each hemispheric emulator (each row) at the beginning, middle, and end of the time series (each column). The black line, y=x, is plotted as a visual guide and represents the ideal case that the distribution of the residuals is perfectly Gaussian.

3.3 Auto-correlation functions

Figure S7 shows the mean auto-correlation functions for the MOZART simulations and the emulator predictions. This figure shows that the emulators are able to replicate the MOZART time correlation structure.
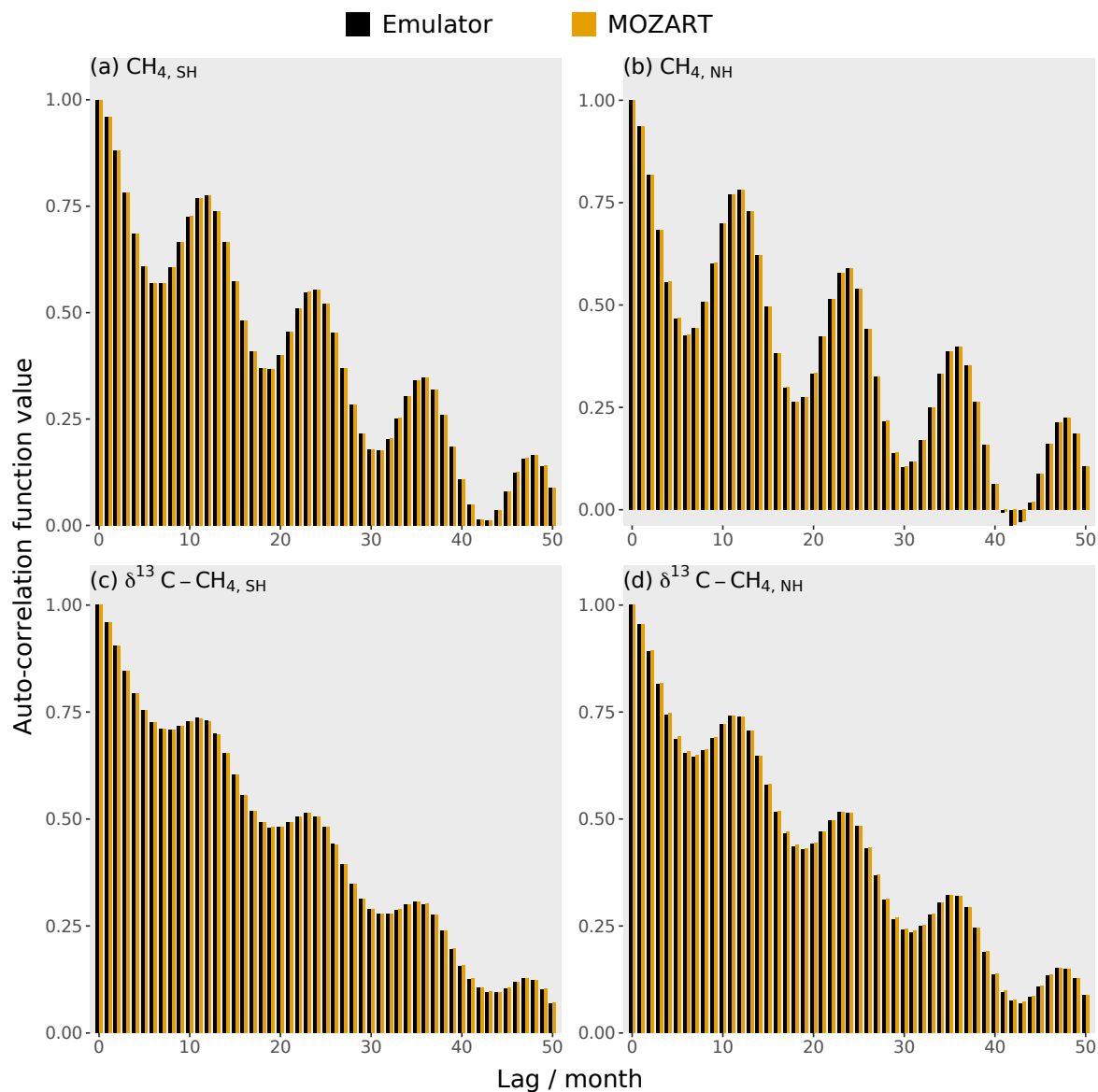
Figure S7: A comparison of the average auto-correlation function: MOZART is shown as the orange bars, and the emulators are shown as the black bars. Each panel shows a different output: (a) the southern hemisphere mole fraction, (b) the northern hemisphere mole fraction, (c) the southern hemisphere δ^{13}C-CH$_4$, and (d) the northern hemisphere δ^{13}C-CH$_4$.

4 NOAA sites used

Table S5 lists all the station locations, where NOAA (Dlugokencky et al., 1994) and INSTAAR (Miller et al., 2002) take measurements, that were used to construct the MOZART monthly median hemispheric outputs emulated in this work. Only grid cells containing stations measuring the methane mole fraction or δ^{13}C-CH$_4$ were included in the hemispheric median for the mole fraction or δ^{13}C-CH$_4$, respectively.

Table S5: All NOAA stations used in this work, along with their latitude, longitude, altitude, and the type of measurement. The units of the altitude data is metres above sea level (masl).

Station	Latitude / ° N	Longitude / ° W	Altitude / masl	Mole fraction	δ^{13}C-CH$_4$
Alert, Nunavut, Canada	82	297	195	x	x
Terceira Island, Azores, Portugal	39	333	24	x	
Baring Head Station, New Zealand	-41	175	90	x	
Tudor Hill, Bermuda, UK	32	295	60	x	
Cold Bay, Alaska, USA	55	197	32	x	
Cape Grim, Tasmania, Australia	-41	145	164	x	x
Crozet Island, France	-46	52	202	x	
Easter Island, Chile	-27	251	57	x	
Mariana Islands, Guam	13	145	7	x	
Halley Station, Antarctica, UK	-76	334	35	x	
Storhofdi, Vestmannaeyjar, Iceland	63	340	127	x	
Izana, Tenerife, Canary Islands	28	344	2378	x	
Key Biscayne, Florida, USA	26	280	6	x	
Cape Kumukahi, Hawaii, USA	20	205	9	x	x
Mace Head, County Galway, Ireland	53	350	26	x	x
Sand Island, Midway, USA	28	183	8	x	
Mauna Loa, Hawaii, USA	20	204	3419	x	x
Niwot Ridge, Colorado, USA	40	254	3526		x
Palmer Station, Antarctica, USA	-65	296	15	x	
Ragged Point, Barbados	13	301	20	x	
Shemya Island, Alaska, USA	53	174	28	x	
Tutuila, American Samoa	-14	189	53	x	x
South Pole, Antarctica, USA	-90	335	2817	x	x
Summit, Greenland	73	322	3215	x	
Syowa Station, Antarctica, Japan	-70	40	16	x	
Tae-ahn Peninsula, Republic of Korea	37	126	21		x
Ushuaia, Argentina	-55	292	32	x	
Mt. Waliguan, People's Republic of China	36	101	3815		x
Ny-Alesund, Svalbard, Norway	79	12	479	x	

5 The number of simulations required to build a useful Gaussian process

The accuracy of the emulators trained with different numbers of simulations was calculated by leave one out cross validation, where each simulation is removed from the training dataset and the emulator predicts the removed simulation. The residuals between the emulator prediction and the training simulation are combined as the temporal average of the root-mean-squared error and are shown in Fig. S8. This figure shows that additional simulations give a diminishing accuracy increase. For many applications, emulators with an error not much smaller than the MOZART invariant parameter error are satisfactory, as the invariant parameter error is an underestimate of the total MOZART error. Therefore, little more than 90 simulations are required.

In general, the number of training simulations required scales linearly with the number of input parameters. However, in a case where a few parameters dominate the output sensitivity, i.e. the problem is of lower dimensionality than it appears, and the relationship between the inputs and output is close to linear, it is possible to train an accurate emulator with fewer simulations than the linear scaling predicts (O'Hagan, 2006). This is demonstrated in the MOZART emulators, and means that Gaussian process emulation could be possible for many complex atmospheric models with a higher spatial resolution than demonstrated in this work.
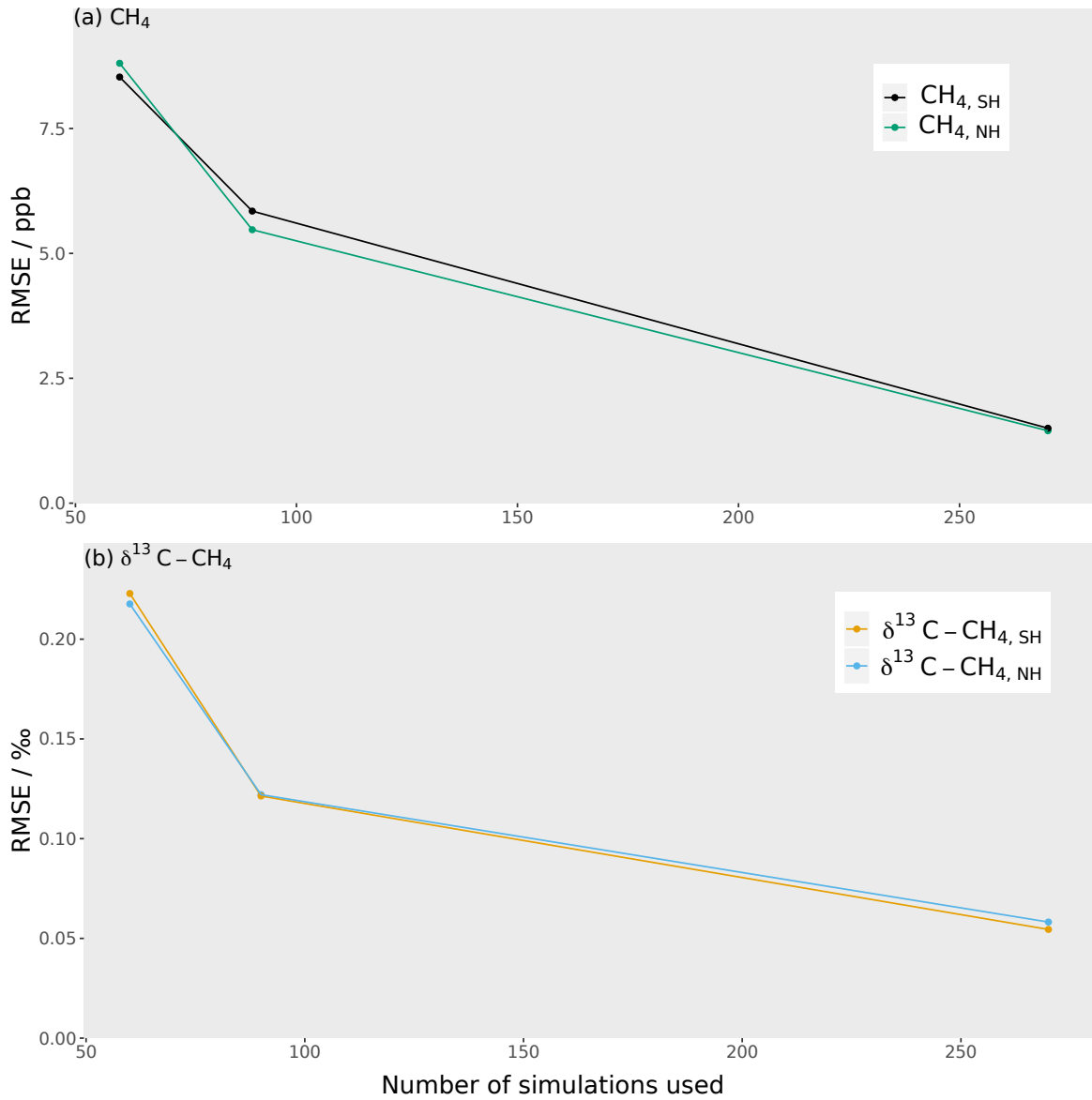
Figure S8: A plot showing how the root-mean-squared error (RMSE) between the emulator and MOZART changes for different numbers of training runs in the emulator. Each measurement type is shown in a separate panel: (a) the mole fraction, with the southern hemisphere in black and the northern hemisphere in green; and (b) δ^{13}C-CH$_4$, with the southern hemisphere in orange and the northern hemisphere in blue.

6 The Monte-Carlo calculation of the sensitivity indices

A $(N, 2k)$ matrix from a Sobol sequence (Sobol', 1967; Antonov and Saleev, 1979) was generated, where N is the number of model simulations ($1\,680\,000$) and k is the number of input parameters (28). This was split into two (N, k) matrices: $\mathbf{A}$ and $\mathbf{B}$. A third matrix $\mathbf{C}_i$, was constructed by replacing the ith column of $\mathbf{B}$ with the ith column of $\mathbf{A}$. The three matrices are input to the emulators to generate

N model outputs each: $\mathbf{y}_A$, $\mathbf{y}_B$, and $\mathbf{y}_{C_i}$. Using these matrices, the first order sensitivity indices can be calculated by

$$S_i = \frac{\frac{1}{N}\sum_{j=1}^{N} \mathbf{y}_A^j \mathbf{y}_{C_i}^j - f_0^2}{\frac{1}{N}\sum_{j=1}^{N} (\mathbf{y}_A^j)^2 - f_0^2},$$

(3)

where

$$f_0^2 = \left(\frac{1}{N}\sum_{j=1}^{N} \mathbf{y}_A^j\right)^2.$$

(4)

The total effect indices can be calculated by

$$S_{T_i} = 1 - \frac{\frac{1}{N}\sum_{j=1}^{N} \mathbf{y}_B^j \mathbf{y}_{C_i}^j - f_0^2}{\frac{1}{N}\sum_{j=1}^{N} (\mathbf{y}_A^j)^2 - f_0^2}.$$

(5)

As suggested in Saltelli et al. (2000), this work uses both $\mathbf{y}_A$ and $\mathbf{y}_B$ instead of just $\mathbf{y}_A$ to calculate f_0^2 and the denominators in Eq. 3 and Eq. 5 (the variance in the output). This improves the accuracy of f_0^2 and the variance in the output, and hence S_i and S_{T_i}, for a fixed N. Uncertainty in these indices was calculated using bootstrap resampling, with 10 000 resamples.

References

Antonov, I. and Saleev, V. (1979), 'An economic method of computing LPτ-sequences', *USSR Computational Mathematics and Mathematical Physics* **19**(1), 243–245. DOI: 10.1016/0041-5553(79)90085-5.

Bastos, L. S. and O'Hagan, A. (2009), 'Diagnostics for gaussian process emulators', *Technometrics* **51**(4), 425–438. DOI: 10.1198/TECH.2009.08019.

Bastviken, D., Cole, J., Pace, M. and Tranvik, L. (2004), 'Methane emissions from lakes: Dependence of lake characteristics, two regional assessments, and a global estimate', *Global Biogeochemical Cycles* **18**(4), GB4009. DOI: 10.1029/2004GB002238.

Cantrell, C. A., Shetter, R. E., McDaniel, A. H., Calvert, J. G., Davidson, J. A., Lowe, D. C., Tyler, S. C., Cicerone, R. J. and Greenberg, J. P. (1990), 'Carbon kinetic isotope effect in the oxidation of methane by the hydroxyl radical', *Journal of Geophysical Research* **95**(D13), 22455–22462. DOI: 10.1029/JD095iD13p22455.

Crowley, J., Saueressig, G., Bergamaschi, P., Fischer, H. and Harris, G. (1999), 'Carbon kinetic isotope effect in the reaction CH4+Cl: a relative rate study using FTIR spectroscopy', *Chemical Physics Letters* **303**(3-4), 268–274. DOI: 10.1016/S0009-2614(99)00243-2.

Davidson, J. A., Cantrell, C. A., Tyler, S. C., Shetter, R. E., Cicerone, R. J. and Calvert, J. G. (1987), 'Carbon kinetic isotope effect in the reaction of CH4 with HO', *Journal of Geophysical Research* **92**(D2), 2195. DOI: 10.1029/jd092id02p02195.

Dlugokencky, E. J., Steele, L. P., Lang, P. M. and Masarie, K. A. (1994), 'The growth rate and distribution of atmospheric methane', *Journal of Geophysical Research* **99**(D8), 17021–17043. DOI: 10.1029/94jd01245.

Gupta, M. L., Mcgrath, M. P., Cicerone, R. J., Rowland, F. S. and Wolfsberg, M. (1997), '12C/13C kinetic isotope effects in the reactions of CH4 with OH and CI', *Geophysical Research Letters* **24**(22), 2761–2764. DOI: 10.1029/97GL02858.

Holgerson, M. A. and Raymond, P. A. (2016), 'Large contribution to inland water CO2 and CH4 emissions from very small ponds', *Nature Geoscience* **9**(3), 222–226. DOI: 10.1038/ngeo2654.

King, S. L., Quay, P. D. and Lansdown, J. M. (1989), 'The 13C/ 12C kinetic isotope effect for soil oxidation of methane at ambient atmospheric concentrations', *Journal of Geophysical Research* **94**(D15), 18273–18277. DOI: 10.1029/JD094iD15p18273.

Kourzeneva, E., Asensio, H., Martin, E. and Faroux, S. (2012), 'Global gridded dataset of lake coverage and lake depth for use in numerical weather prediction and climate modelling', *Tellus, Series A: Dynamic Meteorology and Oceanography* **64**(1), 15640. DOI: 10.3402/tellusa.v64i0.15640.

Lasaga, A. C. and Gibbs, G. V. (1991), 'Ab initio studies of the kinetic isotope effect of the CH4 + OH● atmospheric reaction', *Geophysical Research Letters* **18**(7), 1217–1220. DOI: 10.1029/90GL02679.

Lassey, K. R., Etheridge, D. M., Lowe, D. C., Smith, A. M. and Ferretti, D. F. (2007), 'Centennial evolution of the atmospheric methane budget: What do the carbon isotopes tell us?', *Atmospheric Chemistry and Physics* **7**(8), 2119–2139. DOI: 10.5194/acp-7-2119-2007.

Lehner, B. and Döll, P. (2004), 'Development and validation of a global database of lakes, reservoirs and wetlands', *Journal of Hydrology* **296**(1-4), 1–22. DOI: 10.1016/j.jhydrol.2004.03.028.

Liu, Y. and Boone, D. R. (1991), 'Effects of salinity on methanogenic decomposition', *Bioresource Technology* **35**(3), 271–273. DOI: 10.1016/0960-8524(91)90124-3.

Melissas, V. S. and Truhlar, D. G. (1993), 'Interpolated variational transition state theory and tunneling calculations of the rate constant of the reaction OH+CH4 at 223-2400 K', *The Journal of Chemical Physics* **99**(2), 1013–1027. DOI: 10.1063/1.465401.

Miller, J. B., Mack, K. A., Dissly, R., White, J. W., Dlugokencky, E. J. and Tans, P. P. (2002), 'Development of analytical methods and measurements of 13C/12C in atmospheric CH4 from the NOAA Climate Monitoring and Diagnostics Laboratory Global Air Sampling Network', *Journal of Geophysical Research Atmospheres* **107**(D13), 4178. DOI: 10.1029/2001JD000630.

Natchimuthu, S., Sundgren, I., Gålfalk, M., Klemedtsson, L., Crill, P., Danielsson, Å. and Bastviken, D. (2016), 'Spatio-temporal variability of lake CH 4 fluxes and its influence on annual whole lake emission estimates', *Limnology and Oceanography* **61**(S1), S13–S26. DOI: 10.1002/lno.10222.

O'Hagan, A. (2006), 'Bayesian analysis of computer code outputs: A tutorial', *Reliability Engineering and System Safety* **91**(10-11), 1290–1300. DOI: 10.1016/j.ress.2005.11.025.

Pattnaik, P., Mishra, S. R., Bharati, K., Mohanty, S. R., Sethunathan, N. and Adhya, T. K. (2000), 'Influence of salinity on methanogenesis and associated microflora in tropical rice soils', *Microbiological Research* **155**(3), 215–220. DOI: 10.1016/S0944-5013(00)80035-X.

Reeburgh, W. S., Hirsch, A. I., Sansone, F. J., Popp, B. N. and Rust, T. M. (1997), 'Carbon kinetic isotope effect accompanying microbial oxidation of methane in boreal forest soils', *Geochimica et Cosmochimica Acta* **61**(22), 4761–4767. DOI: 10.1016/S0016-7037(97)00277-9.

Roberto-Neto, O., Coitiño, E. L. and Truhlar, D. G. (1998), 'Dual-level direct dynamics calculations of deuterium and carbon-13 kinetic isotope effects for the reaction Cl + CH4', *Journal of Physical Chemistry A* **102**(24), 4568–4578. DOI: 10.1021/jp980759l.

Rust, F. and Stevens, C. M. (1980), 'Carbon kinetic isotope effect in the oxidation of methane by hydroxyl', *International Journal of Chemical Kinetics* **12**(6), 371–377. DOI: 10.1002/kin.550120602.

Saltelli, A., Ratto, M., Andres, T., Campolongo, F., Cariboni, J., Gatelli, D., Saisana, M. and Tarantola, S. (2000), *Global Sensitivity Analysis: The Primer*, Wiley, Chichester, United Kingdom. DOI: 10.1111/j.1751-5823.2008.00062_17.x.

Saueressig, G., Bergamaschi, P., Crowley, J. N., Fischer, H. and Harris, G. W. (1995), 'Carbon kinetic isotope effect in the reaction of CH4 with Cl atoms', *Geophysical Research Letters* **22**(10), 1225–1228. DOI: 10.1029/95GL00881.

Saueressig, G., Crowley, J. N., Bergamaschi, P., Brühl, C., Brenninkmeijer, C. A. M. and Fischer, H. (2001), 'Carbon 13 and D kinetic isotope effects in the reactions of CH 4 with O(1 D) and OH: New laboratory measurements and their implications for the isotopic composition of stratospheric methane', *Journal of Geophysical Research: Atmospheres* **106**(D19), 23127–23138. DOI: 10.1029/2000JD000120.

Saunois, M., Bousquet, P., Poulter, B., Peregon, A., Ciais, P., Canadell, J. G., Dlugokencky, E. J., Etiope, G., Bastviken, D., Houweling, S., Janssens-Maenhout, G., Tubiello, F. N., Castaldi, S., Jackson, R. B., Alexe, M., Arora, V. K., Beerling, D. J., Bergamaschi, P., Blake, D. R., Brailsford, G., Brovkin, V., Bruhwiler, L., Crevoisier, C., Crill, P., Covey, K., Curry, C., Frankenberg, C., Gedney, N., Höglund-Isaksson, L., Ishizawa, M., Ito, A., Joos, F., Kim, H. S., Kleinen, T., Krummel, P., Lamarque, J. F., Langenfelds, R., Locatelli, R., Machida, T., Maksyutov, S., McDonald, K. C., Marshall, J., Melton, J. R., Morino, I., Naik, V., O'Doherty, S., Parmentier, F. J. W., Patra, P. K., Peng, C., Peng, S., Peters, G. P., Pison, I., Prigent, C., Prinn, R., Ramonet, M., Riley, W. J., Saito, M., Santini, M., Schroeder, R., Simpson, I. J., Spahni, R., Steele, P., Takizawa, A., Thornton, B. F., Tian, H., Tohjima, Y., Viovy, N., Voulgarakis, A., Van Weele, M., Van Der Werf, G. R., Weiss, R., Wiedinmyer, C., Wilton, D. J., Wiltshire, A., Worthy, D., Wunch, D., Xu, X., Yoshida, Y., Zhang, B., Zhang, Z. and Zhu, Q. (2016), 'The global methane budget 2000-2012', *Earth System Science Data* **8**(2), 697–751. DOI: 10.5194/essd-8-697-2016.

Snover, A. K. and Quay, P. D. (2000), 'Hydrogen and carbon kinetic isotope effects during soil uptake of atmospheric methane', *Global Biogeochemical Cycles* **14**(1), 25–39. DOI: 10.1029/1999GB900089.

Sobol', I. (1967), 'On the distribution of points in a cube and the approximate evaluation of integrals', *USSR Computational Mathematics and Mathematical Physics* **7**(4), 86–112. DOI: 10.1016/0041-5553(67)90144-9.

Stell, A. C. (2020), 'Global methane freshwater emission map for atmospheric modelling'. DOI: 10.17605/OSF.IO/Q9F8P.
URL: *https://osf.io/q9f8p/*

Tanaka, N., Xiao, Y., Hatakeyama, S. and Ueda, S. (1997), Determination of carbon KIE of CH4 + CI reaction: Large reaction chamber experiment and its implications to atmospheric methane chemistry, *in* 'EOS Trans. Amer. Geophys. Union, 78, Sprint Meeting Suppl., S75'.

Tyler, S. C., Ajie, H. O., Rice, A. L. and Cicerone, R. J. (2000), 'Experimentally determined kinetic isotope effects in the reaction of CH4 with Cl: Implications for atmospheric CH4', *Geophysical Research Letters* **27**(12), 1715–1718. DOI: 10.1029/1999GL011168.

Tyler, S. C., Crill, P. M. and Brailsford, G. W. (1994), '13C/12C Fractionation of methane during oxidation in a temperate forested soil', *Geochimica et Cosmochimica Acta* **58**(6), 1625–1633. DOI: 10.1016/0016-7037(94)90564-9.

Verpoorter, C., Kutser, T., Seekell, D. A. and Tranvik, L. J. (2014), 'A global inventory of lakes based on high-resolution satellite imagery', *Geophysical Research Letters* **41**(18), 6396–6402. DOI: 10.1002/2014GL060641.

Wik, M., Thornton, B. F., Bastviken, D., Uhlbäck, J. and Crill, P. M. (2016), 'Biased sampling of methane release from northern lakes: A problem for extrapolation', *Geophysical Research Letters* **43**(3), 1256–1262. DOI: 10.1002/2015GL066501.

Wik, M., Varner, R. K., Anthony, K. W., MacIntyre, S. and Bastviken, D. (2016), 'Climate-sensitive northern lakes and ponds are critical components of methane release', *Nature Geoscience* **9**(2), 99–105. DOI: 10.1038/ngeo2578.

Wilkinson, J., Maeck, A., Alshboul, Z. and Lorke, A. (2015), 'Continuous Seasonal River Ebullition Measurements Linked to Sediment Methane Formation', *Environmental Science & Technology* **49**(22), 13121–13129. DOI: 10.1021/acs.est.5b01525.